Published in final edited form as:
Biomaterials. 2013 April ; 34(12): 3002–3009. doi:10.1016/j.biomaterials.2013.01.047.

Tumor Vasculature Targeting and Imaging in Living Mice with Reduced Graphene Oxide

Sixiang Shi[1], **Kai Yang**[2], **Hao Hong**[3], **Hector F. Valdovinos**[4], **Tapas R. Nayak**[3], **Yin Zhang**[4], **Charles P. Theuer**[5], **Todd E. Barnhart**[4], **Zhuang Liu**[2], and **Weibo Cai**[1,3,4,6,*]

[1]Materials Science Program, University of Wisconsin - Madison, WI, USA

[2]Jiangsu Key Laboratory for Carbon-Based Functional Materials and Devices, Institute of Functional Nano and Soft Materials Laboratory (FUNSOM), Soochow University, Suzhou, Jiangsu, China

[3]Department of Radiology, University of Wisconsin - Madison, WI, USA

[4]Department of Medical Physics, University of Wisconsin - Madison, WI, USA

[5]TRACON Pharmaceuticals, Inc., San Diego, CA, USA

[6]University of Wisconsin Carbone Cancer Center, Madison, WI, USA

Abstract

Graphene-based nanomaterials have attracted tremendous attention in the field of biomedicine due to their intriguing properties. Herein, we report tumor vasculature targeting and imaging in living mice using reduced graphene oxide (RGO), which was conjugated to the anti-CD105 antibody TRC105. The RGO conjugate, ^{64}Cu-NOTA-RGO-TRC105, exhibited excellent stability in vitro and in vivo. Serial positron emission tomography (PET) imaging studies non-invasively assessed the pharmacokinetics and demonstrated specific targeting of ^{64}Cu-NOTA-RGO-TRC105 to 4T1 murine breast tumors in vivo, compared to non-targeted RGO conjugate (^{64}Cu-NOTA-RGO). In vivo (e.g., blocking 4T1 tumor uptake with excess TRC105), in vitro (e.g., flow cytometry), and ex vivo (e.g., histology) experiments confirmed the specificity of ^{64}Cu-NOTA-RGO-TRC105 for tumor vascular CD105. Since RGO exhibits desirable properties for photothermal therapy, the tumor-specific RGO conjugate developed in this work may serve as a promising theranostic agent that integrates imaging and therapeutic components.

Keywords

reduced graphene oxide (RGO); cancer; positron emission tomography (PET); tumor angiogenesis; CD105 (endoglin); nanomedicine

1. Introduction

Graphene, an intriguing nanomaterial with unique mechanical, electronic, optical, and chemical properties, has attracted tremendous interest over the last several years [1–6]. Ultrahigh surface area, excellent electrical conductivity, ideal photothermal property, versatile chemistry, and low toxicity allow graphene-based nanomaterials to have applications in biosensing, tissue engineering, drug and gene delivery, molecular imaging, photothermal therapy, among others [7–10]. Potential toxicity is a major concern for in vivo

Corresponding Author: Weibo Cai, PhD, Departments of Radiology and Medical Physics, University of Wisconsin - Madison, Room 7137, 1111 Highland Ave, Madison, WI 53705-2275, USA. wcai@uwhealth.org; Phone: 608-262-1749; Fax: 608- 265-0614.

applications of nanomaterials. Recently, we demonstrated that various graphene-based nanomaterials do not render noticeable toxicity in animals after polyethylene glycol (PEG) modification [11, 12], which warranted further in vivo investigation of graphene-based nanomaterials.

An emerging strategy for the development of new anti-cancer therapies is to harness the potential of nanotechnology to improve the therapeutic efficacy [13–15]. Among the different subtypes of graphene-based nanomaterials, reduced graphene oxide (RGO) is an excellent photothermal agent that enables highly efficient in vivo tumor ablation [12]. In addition, RGO can be used to integrate imaging and therapeutic components for cancer theranostics [16]. Despite the many desirable properties for biomedical applications, the use of RGO conjugates for in vivo tumor targeting has not been reported, which is the focus of this study.

The size of nanomaterials is a significant barrier for extravasation, which limits the use of various nanomaterials for tumor targeting, imaging, and therapy [17–19]. We believe tumor vasculature instead of tumor cell targeting is more desirable for graphene-based nanomaterials, since the targets are immediately accessible upon intravenous injection and extravasation is not required to achieve tumor targeting/contrast. Furthermore, angiogenesis (i.e., new blood vessel formation) is a critical process in tumor development and metastasis, hence is applicable to all solid tumors [20]. CD105 (i.e., endoglin) is almost exclusively expressed on proliferating tumor endothelial cells, which serves as an ideal vascular target [21–23]. More importantly, the expression level of CD105 is correlated with poor prognosis in more than 10 solid tumor types [24], which makes it a generally applicable prognostic, diagnostic, and therapeutic vascular target in cancer. TRC105, a human/murine chimeric IgG1 monoclonal antibody which binds to both human and murine CD105 [25], was used as the targeting ligand in this work.

The goal of this study was to investigate in vivo tumor vasculature targeting with TRC105-conjugated RGO, which can be non-invasively and quantitatively measured with serial positron emission tomography (PET) imaging. Since PET is widely used in clinical oncology [26–29], the incorporation of a PET isotope in the RGO conjugates can facilitate future translation of graphene-based nanomaterials. PEG chains (5 kDa) were used to modify the surface of RGO for enhanced in vivo stability and biocompatibility, with amine groups at the terminal end for covalent conjugation of various functional entities. ^{64}Cu (half-life: 12.7 h) was used as the PET label, with 1,4,7-triazacyclononane-1,4,7-triacetic acid (NOTA) as the chelator. To demonstrate CD105 specificity of TRC105-conjugated RGO, various in vitro, in vivo, and ex vivo experiments were carried out.

2. Materials and methods

2.1. Reagents

TRC105 was provided by TRACON Pharmaceuticals Inc. (San Diego, CA). S-2-(4-isothiocyanatobenzyl)-1,4,7-triazacyclononane-1,4,7-triacetic acid (p-SCN-Bn-NOTA) was purchased from Macrocyclics, Inc. (Dallas, TX). Chelex 100 resin (50–100 mesh) and fluorescein isothiocyanate (FITC) were purchased from Sigma-Aldrich (St. Louis, MO). Succinimidyl carboxymethyl PEG maleimide (SCM-PEG-Mal; molecular weight: 5 kDa; Creative PEGworks, Winston Salem, NC), rat anti-mouse CD31 primary antibody (BD Biosciences, San Diego, CA), AlexaFluor488- or Cy3-labeled secondary antibodies (Jackson Immunoresearch Laboratories, Inc., West Grove, CA), and PD-10 desalting columns (GE Healthcare, Piscataway, NJ) were all acquired from commercial sources. Water and all buffers were of Millipore grade and pre-treated with Chelex 100 resin to

ensure that the aqueous solution was free of heavy metal. All other reaction buffers and chemicals were obtained from Thermo Fisher Scientific (Fair Lawn, NJ).

2.2. Syntheses of the RGO conjugates

RGO-PEG-NH_2 was prepared in a similar fashion as detailed in our previous report [12]. In brief, PEG grafted poly(maleic anhydride-alt-1-octadecene) (abbreviated as C_{18}PMH-PEG_{5000}-NH_2) was synthesized following our previously reported procedure [30]. A 3:1 ratio of mPEG-NH_2 (5 kDa, PEG Bio, China) and Boc-NH-PEG-NH_2 (5 kDa, IRIS Biotech GmbH, Germany) was used to react with C_{18}PMH, obtaining C_{18}PMH-PEG_{5000}-NH_2 after deprotection of the Boc group with trifluoroacetic acid. The C_{18}PMH-PEG_{5000}-NH_2 solution was dialyzed against water using a 14 kDa molecular weight cut-off (MWCO) membrane and then lyophilized. To functionalize RGO via hydrophobic interactions between the C_{18} chains and the RGO surface, 10 mg of C_{18}PMH-PEG_{5000}-NH_2 was mixed with 1 mg of RGO and sonicated for 90 min to yield RGO-PEG-NH_2 (Figure 1A). The suspension was centrifuged at 14,800 rpm for 3 h to remove any unstable aggregates. The supernatant was collected and washed through 100 nm filter membrane to remove excess C_{18}PMH-PEG_{5000}-NH_2.

RGO-PEG-NH_2 was mixed with p-SCN-Bn-NOTA or FITC, which has the same chemical reaction between the SCN group and the NH_2 group on RGO, at a molar ratio of 1:10 at pH 9.0 for 2 h. The resulting NOTA-RGO (or FITC-RGO) was purified by centrifugation with 100 kDa MWCO Amicon filters at 8,000 rpm for 15 min. Of note, most NH_2 groups are still present on the surface of NOTA-RGO and FITC-RGO for further functionalization with SCM-PEG-Mal. Subsequently, NOTA-RGO (or FITC-RGO) was reacted with SCM-PEG-Mal at a molar ratio of 1:30 at pH 8.5 for 2 h. The resulting NOTA-RGO-PEG-Mal or FITC-RGO-PEG-Mal was purified by centrifugation with 100 kDa MWCO Amicon filters at 8,000 rpm for 15min.

TRC105 was incubated with Traut's reagent at a molar ratio of 1:25 at pH 8.0 for 2 h. The resulting TRC105-SH was purified by size exclusion column chromatography with phosphate-buffered saline (PBS, pre-treated with Chelex 100 resin to prevent oxidation of the thiol) as the mobile phase. Afterwards, NOTA-RGO-PEG-Mal (or FITC-RGO-PEG-Mal) was reacted with TRC105-SH at a molar of 1:5 at pH 7.5 in the presence of tris(2-carboxyethyl)phosphine (TCEP, to prevent oxidation of the thiol). The final products were purified by size exclusion column chromatography and termed as NOTA-RGO-TRC105 or FITC-RGO-TRC105.

Although all the RGO conjugates (i.e., NOTA-RGO-TRC105, FITC-RGO-TRC105, NOTA-RGO, and FITC-RGO) have PEG chains on the surface, the term "PEG" was not included in the names for brevity consideration. Scanning electron microscopy (SEM), atomic force microscopy (AFM), dynamic light scattering (DLS), and zeta-potential measurements were performed to characterize the RGO conjugates.

2.3. Cell lines and animal model

4T1 murine breast cancer, MCF-7 human breast cancer, and human umbilical vein endothelial cells (HUVECs) were obtained from the American Type Culture Collection (ATCC, Manassas, VA) and cultured as previously described [31–33]. Cells were used for in vitro and in vivo experiments when they reached ~80% confluence. All animal studies were conducted under a protocol approved by the University of Wisconsin Institutional Animal Care and Use Committee. Four- to five-week-old female BALB/c mice (Harlan, Indianapolis, IN) were each injected with 2×10^6 4T1 cells in the flank to generate the 4T1

breast cancer model. The mice were used for in vivo experiments when the tumor diameter reached 6–8 mm.

2.4. Flow cytometry

HUVECs (CD105 positive) and MCF-7 (CD105 negative) cells [31, 34] were harvested and suspended in cold PBS with 2% bovine serum albumin at a concentration of 5×10^6 cells/mL, incubated with FITC-RGO-TRC105 or FITC-RGO at a concentration of 50 μg/mL (based on RGO) for 30 min at room temperature, centrifuged at 1,000 rpm for 5 min, and washed three times with cold PBS. To further evaluate CD105 specificity of FITC-RGO-TRC105, a blocking experiment was carried out where 500 μg/mL of TRC105 was added to the incubated cells. Subsequently, the cells were analyzed using a BD FACSCalibur 4-color analysis cytometer equipped with 488 nm and 633 nm lasers (Becton-Dickinson, San Jose, CA) and FlowJo analysis software (Tree Star, Inc., Ashland, OR).

2.5. ^{64}Cu-labeling and serum stability studies

^{64}Cu was produced with an onsite cyclotron (GE PETrace). $^{64}CuCl_2$ (74 MBq) was diluted in 300 μL of 0.1 M sodium acetate buffer (pH 6.5) and mixed with 50 μg of NOTA-RGO-TRC105 or NOTA-RGO. The reaction was conducted at 37 °C for 30 min with constant shaking. The resulting ^{64}Cu-NOTA-RGO-TRC105 or ^{64}Cu-NOTA-RGO was purified by size exclusion column chromatography using PBS as the mobile phase. The radioactive fractions containing ^{64}Cu-NOTA-RGO-TRC105 or ^{64}Cu-NOTA-RGO were collected for further in vitro and in vivo studies.

To ensure that ^{64}Cu-NOTA-RGO-TRC105 and ^{64}Cu-NOTA-RGO are sufficiently stable for in vivo applications, serum stability studies were carried out. ^{64}Cu-NOTA-RGO-TRC105 or ^{64}Cu-NOTA-RGO were incubated in complete mouse serum at 37 °C for up to 48 h. Portions of the mixture were sampled at different time points and filtered through 100 kDa MWCO filters. The radioactivity within the filtrate was measured, and the percentages of retained (i.e., intact) ^{64}Cu on the RGO conjugates (^{64}Cu-NOTA-RGO-TRC105 or ^{64}Cu-NOTA-RGO) were calculated using the equation (total radioactivity - radioactivity in filtrate)/total radioactivity × 100%.

2.6. PET imaging and biodistribution studies

PET scans of 4T1 tumor-bearing mice (4 mice per group), at various time points post-injection (p.i.) of 5–10 MBq of ^{64}Cu-NOTA-RGO-TRC105 or ^{64}Cu-NOTA-RGO via tail vein, were performed using a microPET/microCT Inveon rodent model scanner (Siemens Medical Solutions USA, Inc.). Detailed procedures for data acquisition, image reconstruction, and region-of-interest (ROI) analysis of the PET data have been reported previously [32, 35]. Quantitative PET data of the 4T1 tumor and major organs were presented as percentage injected dose per gram of tissue (%ID/g).

To confirm in vivo CD105 specificity of ^{64}Cu-NOTA-RGO-TRC105, another group of four 4T1 tumor-bearing mice were each injected with 1 mg of TRC105 at 2 h before ^{64}Cu-NOTA-RGO-TRC105 administration and subsequent serial PET imaging. To validate that the %ID/g values based on PET imaging accurately reflected the radioactivity distribution in tumor-bearing mice, biodistribution studies were conducted at 48 h p.i. (at the end of serial PET scans) and 3 h p.i. (when the tumor uptake was at the peak, using a separate cohort of four mice). Mice were euthanized and blood, 4T1 tumor, and major organs/tissues were collected and wet-weighed. The radioactivity in the tissue was measured using a γ counter (PerkinElmer) and presented as %ID/g (mean ± SD).

2.7. Histology

A group of three 4T1 tumor-bearing mice was each injected with NOTA-RGO-TRC105 (5 mg/kg of mouse body weight) and euthanized at 3 h p.i. (when 4T1 tumor uptake was at the peak based on PET imaging). The 4T1 tumor, liver, spleen (which has high uptake of ^{64}Cu-NOTA-RGO-TRC105), and muscle (which has low uptake of ^{64}Cu-NOTA-RGO-TRC105 and serves as a control normal organ) were frozen and cryo-sectioned for histological analysis.

Frozen tissue slices of 7 μm thickness were fixed with cold acetone and stained for endothelial marker CD31, as described previously through the use of a rat anti-mouse CD31 antibody and a Cy3-labeled donkey anti-rat IgG [31, 32]. The tissue slices were also incubated with 2 μg/mL of AlexaFluor488-labeled goat anti-human IgG for visualization of NOTA-RGO-TRC105 (i.e., TRC105 within the NOTA-RGO-TRC105 conjugate served as a primary antibody and no additional TRC105 was used for histology studies). All images were acquired with a Nikon Eclipse Ti microscope.

3. Results

3.1. Syntheses and characterization of the RGO conjugates

A schematic structure of the RGO conjugates is shown in Figure 1A. Based on SEM and AFM measurements, RGO-PEG-NH_2, NOTA-RGO, and NOTA-RGO-TRC105 exist as small sheets within a size range of 20–80 nm (Figure 1B,C). DLS measurement showed that RGO-PEG-NH_2 has a hydrodynamic diameter of 22.3 ± 3.2 nm, whereas the diameter of NOTA-RGO and NOTA-RGO-TRC105 are 26.2 ± 3.6 nm and 37.0 ± 7.2 nm, respectively. The zeta-potential value of RGO-PEG-NH_2 was −20.3 ± 1.6 mV (which is expected since there are more $–COO^-$ on the RGO surface than $–NH_3^+$). After further conjugation, the zeta-potential values changed significantly to −16.4 ± 4.6 mV (NOTA-RGO) and −2.0 ± 5.2 mV (NOTA-RGO-TRC105), suggesting successful conjugation of NOTA and TRC105 onto the surface of RGO.

3.2. Flow cytometry and serum stability studies

As evidenced in Figure 2A, the fluorescence signal of CD105 positive HUVECs was significantly enhanced (~25 fold higher than the untreated cells) upon incubation with FITC-RGO-TRC105, whereas no fluorescence enhancement was observed after blocking (with TRC105) or upon FITC-RGO treatment. On CD105 negative MCF-7 cells, the fluorescence signal was minimal for all groups. Taken together, flow cytometry results indicated high CD105 specificity and minimal non-specific binding of TRC105-conjugated RGO in cell culture.

Serum stability studies confirmed that ^{64}Cu-NOTA-RGO-TRC105 and ^{64}Cu-NOTA-RGO are highly stable for in vivo applications. Nearly 90% of ^{64}Cu remained on the RGO conjugates after incubation in complete mouse serum at 37 °C for 48 h (Figure 2B), indicating excellent stability of the radiolabel (i.e., ^{64}Cu) on NOTA-RGO and NOTA-RGO-TRC105. Since PET imaging detects the radiolabel rather than the RGO conjugates per se, excellent stability of the radiolabel on the RGO conjugates ensures that the signal observed with PET imaging truly reflects distribution of the RGO conjugates.

3.3. PET and biodistribution studies

^{64}Cu has a 12.7 h decay half-life. Therefore, the time points of 0.5, 3, 6, 16, 24 and 48 h p.i. were chosen for serial PET scans in 4T1 tumor-bearing mice. The coronal PET images that contain the 4T1 tumors are shown in Figure 3, and the quantitative data obtained from ROI analysis of the PET data are shown in Figure 4.

Since the size of RGO conjugates is significantly larger than the cutoff for renal filtration (~5 nm) [36], they were cleared from mice mainly through the hepatobiliary pathway. The liver uptake of ^{64}Cu-NOTA-RGO-TRC105 was 18.3 ± 2.8, 16.7 ± 0.9, 16.7 ± 2.0, 13.4 ±1.0, 13.5 ± 0.9, and 11.5 ± 0.5 %ID/g at 0.5, 3, 6, 16, 24, and 48 h p.i. respectively, while the radioactivity in the blood was 4.6 ± 1.6, 3.6 ± 0.4, 3.7 ± 0.5, 3.2 ± 0.1, 3.1 ± 0.1, and 2.9 ± 0.1 %ID/g at 0.5, 3, 6, 16, 24, and 48 h p.i. respectively (n = 4; Figure 4A), indicating a short circulation half-life (< 30 min). Importantly, the 4T1 tumor uptake of ^{64}Cu-NOTA-RGO-TRC105 was clearly visible at 0.5 h p.i. (Figure 3) and remained stable over time (5.0 ± 0.6, 5.6 ± 0.2, 5.7 ± 0.2, 4.8 ± 0.3, 4.5 ± 0.4, and 4.0 ± 0.5 %ID/g at 0.5, 3, 6, 16, 24, and 48 h p.i. respectively; n = 4; Figure 4A,D), which provided excellent tumor contrast.

Pre-injection of a blocking dose of TRC105 significantly reduced the 4T1 tumor uptake of ^{64}Cu-NOTA-RGO-TRC105 to 2.1 ± 0.4, 2.2 ± 0.3, 2.4 ± 0.3, 2.4 ± 0.3, 2.5 ± 0.2, and 2.4 ± 0.3 %ID/g at 0.5, 3, 6, 16, 24, and 48 h p.i. respectively (n = 4; Figure 3, 4B,D; $P < 0.05$ at all time points when compared to mice injected with ^{64}Cu-NOTA-RGO-TRC105 alone), which demonstrated in vivo specificity of ^{64}Cu-NOTA-RGO-TRC105 for CD105 expressed by proliferating tumor vasculature. Radioactivity uptake of the liver in the group pre-injected with a blocking dose of TRC105 was similar to mice injected with ^{64}Cu-NOTA-RGO-TRC105 alone, which were 15.6 ± 1.8, 14.4 ± 1.3, 12.7 ± 1.6, 9.9 ± 1.3, 9.7 ± 1.1, and 7.8 ± 1.2 %ID/g at 0.5, 3, 6, 16, 24, and 48 h p.i. respectively (n = 4; Figure 4B). Radioactivity in the blood (2.8 ± 0.1, 2.9 ± 0.3, 3.3 ± 0.3, 3.4 ± 0.3, 3.3 ± 0.2, and 3.0 ± 0.4 %ID/g at 0.5, 3, 6, 16, 24, and 48 h p.i. respectively; n = 4; Figure 4B) was slightly affected by the blocking dose of TRC105 (i.e., lower blood radioactivity at early time points).

The 4T1 tumor uptake of ^{64}Cu-NOTA-RGO (3.4 ± 1.2, 2.7 ± 0.9, 3.1 ± 1.0, 2.2 ± 0.7, 2.0 ± 0.6, and 1.7 ± 0.3 %ID/g at 0.5, 3, 6, 16, 24, and 48 h p.i. respectively; n = 4; Figure 4C,D) was ~2 fold lower than that of ^{64}Cu-NOTA-RGO-TRC105 ($P < 0.05$ at all time points except 0.5 h p.i.), indicating that conjugation of TRC105 to RGO markedly increased tumor uptake through active targeting of CD105 on the tumor vasculature. Liver uptake (17.9 ± 5.0, 13.9 ± 2.9, 14.3 ± 3.2, 10.4 ± 2.3, 10.4 ± 2.0, and 8.2 ± 1.5 %ID/g at 0.5, 3, 6, 16, 24, and 48 h p.i. respectively; n = 4; Figure 4C) and radioactivity in the blood (2.9 ± 0.2, 2.4 ± 0.6, 2.5 ± 0.6, 2.2 ± 0.6, 2.2 ± 0.6, and 1.9 ± 0.6 %ID/g at 0.5, 3, 6, 16, 24, and 48 h p.i. respectively; n = 4; Figure 4C) for ^{64}Cu-NOTA-RGO were similar as those of mice injected with ^{64}Cu-NOTA-RGO-TRC105.

Biodistribution studies were carried out at 3 h p.i. (Figure 5A, when tumor uptake was at the peak based on PET imaging) and 48 h p.i. (Figure 5B, following the last PET scans) to validate the PET results. Overall, the quantitative results based on PET and biodistribution studies matched very well, confirming that serial non-invasive PET imaging accurately reflected the distribution of ^{64}Cu-NOTA-RGO-TRC105 and ^{64}Cu-NOTA-RGO in tumor-bearing mice. Because of uptake in the reticuloendothelial system (RES) and hepatobiliary clearance which is commonly observed for intravenously injected nanomaterials, substantial radioactivity was detected in the liver, spleen, and intestine. Importantly, even at 48 h p.i., the tumor uptake of ^{64}Cu-NOTA-RGO-TRC105 was significantly higher than that of ^{64}Cu-NOTA-RGO and the blocking group, indicating that vascular CD105 targeting with TRC105 as the ligand could effectively enhance the tumor uptake in vivo.

3.4. Histology

Histological studies were carried out to confirm that ^{64}Cu-NOTA-RGO-TRC105 was successfully delivered to the tumor vasculature via CD105 targeting, which serves as a critical cross-validation of the in vivo results since PET only measures the distribution of ^{64}Cu but not the RGO conjugate per se. As indicated in Figure 6, NOTA-RGO-TRC105 distribution in the 4T1 tumor was primary on the vasculature (indicated by excellent overlay

of the red and green fluorescence signal, which represents CD31 and NOTA-RGO-TRC105, respectively).

Due to the relatively large size of NOTA-RGO-TRC105, little extravasation (i.e., green spots in the merged image) was observed in the 4T1 tumor which confirmed that tumor vasculature targeting is a valid and suitable approach for RGO. On the other hand, the green fluorescence (attributed to NOTA-RGO-TRC105) in the liver and spleen was mostly outside the vasculature (red fluorescence for CD31 staining), suggesting that NOTA-RGO-TRC105 was captured by liver and spleen through non-specific RES uptake instead of CD105 targeting. Little green fluorescence was observed in the muscle, which is consistent with the results of PET and biodistribution studies.

4. Discussion

The results from this work are significant in several aspects. First, active tumor targeting in living subjects with RGO has not been reported to date, although in vitro tumor cell targeting has been investigated [37]. The improved tumor uptake of ^{64}Cu-NOTA-RGO-TRC105 via tumor vascular CD105 targeting could be utilized for tumor-targeted drug delivery and/or photothermal therapy of cancer, to enhance therapeutic efficacy and enable cancer theranostics. Of note, RGO has more desirable properties for photothermal therapy than graphene oxide (GO, which is more hydrophilic and used in our previous studies [31, 34]) because of its strong absorbance in the near-infrared range [12, 16, 37]. Second, PET has been widely used in clinical oncology for cancer staging and monitoring the therapeutic response [26, 28, 38, 39]. The wide availability of dedicated small animal PET scanners and clinical PET scanners can enable non-invasive imaging and quantitation of the uptake of RGO conjugates in small animal tumor models and facilitate clinical translation.

Third, robust chemistry for RGO functionalization is of utmost importance to future biomedical applications. In vivo stability of the radiolabel is critical for imaging applications. In this regard, the stability of NOTA as a chelator for ^{64}Cu has been well documented in the literature [40, 41]. In addition, the excellent stability for surface conjugation of carbon-based nanomaterials via hydrophobic interactions (e.g., with C_{18} chains) has been well documented in multiple previous reports [12, 16, 30, 37, 42], and was confirmed in our serum stability studies (Figure 2B) and corroborated by ex vivo histology (Figure 6).

For in vivo tumor targeting using nanomaterials such as RGO, vasculature targeting is a promising approach since many nanomaterials extravasate poorly [43–46]. CD105 is a receptor primarily expressed on tumor neovasculature, independent of its expression on tumor cells [21, 23, 24], and thus can serve as a universal target for multiple solid tumor types. 4T1 breast cancer is a highly vascularized tumor model that grows rapidly upon implantation and provides a sufficient number of vessels for in vivo imaging of angiogenesis (microvessel density of the 4T1 tumor was 205 ± 29 vessels/mm^2 based on CD105 histology; n = 8), while the 4T1 cells themselves do not express significant level of CD105 [32, 34]. Since the 4T1 tumor uptake of ^{64}Cu-NOTA-RGO-TRC105 peaked at 3–6 h p.i., the use of shorter lived PET isotopes (e.g., ^{61}Cu which has a decay half-life of 3.3 h) [10] may also suffice in future studies. Research using graphene-based nanomaterials (especially in their biomedical applications) is still at a nascent stage due to the short time span since the initial report in 2004 [1]. This study serves as an important proof-of-principle for the use of RGO for in vivo tumor vasculature targeting.

5. Conclusion

Herein we report in vivo tumor vasculature targeting of RGO in a breast cancer model, with ^{64}Cu as the PET label and TRC105 as the targeting ligand. CD105 (the target of TRC105) is specifically and densely expressed on proliferating tumor endothelial cells of many solid tumor types, making it suitable for nanomaterial-based tumor targeting. The RGO conjugates exhibited excellent stability and high specificity for CD105, based on various in vivo/in vitro/ex vivo studies. Serial PET imaging revealed rapid tumor uptake of ^{64}Cu-NOTA-RGO-TRC105, which peaked at 3 h p.i. and remained stable over time. Importantly, ^{64}Cu-NOTA-RGO-TRC105 exhibited little extravasation in the 4T1 tumor, indicating that tumor vasculature (instead of tumor cell) targeting is a valid and preferred approach for nanomaterials.

Acknowledgments

This work is supported, in part, by the University of Wisconsin Carbone Cancer Center, the Department of Defense (W81XWH-11-1-0644), the Elsa U. Pardee Foundation, the National Basic Research Program of China (973 Program, 2012CB932601 & 2011CB911002), and the National Science Foundation of China (51002100 & 51222203).

References

1. Novoselov KS, Geim AK, Morozov SV, Jiang D, Zhang Y, Dubonos SV, et al. Electric field effect in atomically thin carbon films. Science. 2004; 306:666–9. [PubMed: 15499015]
2. Geim AK, Novoselov KS. The rise of graphene. Nat Mater. 2007; 6:183–91. [PubMed: 17330084]
3. Service RF. Materials science. Carbon sheets an atom thick give rise to graphene dreams. Science. 2009; 324:875–7. [PubMed: 19443761]
4. Pumera M. Graphene-based nanomaterials and their electrochemistry. Chem Soc Rev. 2010; 39:4146–57. [PubMed: 20623061]
5. Li X, Wang X, Zhang L, Lee S, Dai H. Chemically derived, ultrasmooth graphene nanoribbon semiconductors. Science. 2008; 319:1229–32. [PubMed: 18218865]
6. Huang X, Yin Z, Wu S, Qi X, He Q, Zhang Q, et al. Graphene-based materials: synthesis, characterization, properties, and applications. Small. 2011; 7:1876–902. [PubMed: 21630440]
7. Novoselov KS, Fal'ko VI, Colombo L, Gellert PR, Schwab MG, Kim K. A roadmap for graphene. Nature. 2012; 490:192–200. [PubMed: 23060189]
8. Feng L, Liu Z. Graphene in biomedicine: opportunities and challenges. Nanomedicine (Lond). 2011; 6:317–24. [PubMed: 21385134]
9. Yang K, Feng L, Shi X, Liu Z. Nano-graphene in biomedicine: theranostic applications. Chem Soc Rev. 2012; 42:530–47. [PubMed: 23059655]
10. Zhang Y, Nayak TR, Hong H, Cai W. Graphene: a versatile nanoplatform for biomedical applications. Nanoscale. 2012; 4:3833–42. [PubMed: 22653227]
11. Yang K, Wan J, Zhang S, Zhang Y, Lee ST, Liu Z. In vivo pharmacokinetics, long-term biodistribution, and toxicology of PEGylated graphene in mice. ACS Nano. 2011; 5:516–22. [PubMed: 21162527]
12. Yang K, Wan J, Zhang S, Tian B, Zhang Y, Liu Z. The influence of surface chemistry and size of nanoscale graphene oxide on photothermal therapy of cancer using ultra-low laser power. Biomaterials. 2012; 33:2206–14. [PubMed: 22169821]
13. Davis ME, Chen ZG, Shin DM. Nanoparticle therapeutics: an emerging treatment modality for cancer. Nat Rev Drug Discov. 2008; 7:771–82. [PubMed: 18758474]
14. Torchilin VP. Recent advances with liposomes as pharmaceutical carriers. Nat Rev Drug Discov. 2005; 4:145–60. [PubMed: 15688077]
15. Peer D, Karp JM, Hong S, Farokhzad OC, Margalit R, Langer R. Nanocarriers as an emerging platform for cancer therapy. Nat Nanotechnol. 2007; 2:751–60. [PubMed: 18654426]

16. Yang K, Hu L, Ma X, Ye S, Cheng L, Shi X, et al. Multimodal imaging guided photothermal therapy using functionalized graphene nanosheets anchored with magnetic nanoparticles. Adv Mater. 2012; 24:1868–72. [PubMed: 22378564]

17. Ruoslahti E, Bhatia SN, Sailor MJ. Targeting of drugs and nanoparticles to tumors. J Cell Biol. 2010; 188:759–68. [PubMed: 20231381]

18. Cai W, Chen X. Nanoplatforms for targeted molecular imaging in living subjects. Small. 2007; 3:1840–54. [PubMed: 17943716]

19. Hong H, Zhang Y, Sun J, Cai W. Molecular imaging and therapy of cancer with radiolabeled nanoparticles. Nano Today. 2009; 4:399–413. [PubMed: 20161038]

20. Hanahan D, Weinberg RA. The hallmarks of cancer. Cell. 2000; 100:57–70. [PubMed: 10647931]

21. Seon BK, Haba A, Matsuno F, Takahashi N, Tsujie M, She X, et al. Endoglin-targeted cancer therapy. Curr Drug Deliv. 2011; 8:135–43. [PubMed: 21034418]

22. Fonsatti E, Nicolay HJ, Altomonte M, Covre A, Maio M. Targeting cancer vasculature via endoglin/CD105: a novel antibody-based diagnostic and therapeutic strategy in solid tumours. Cardiovasc Res. 2010; 86:12–9. [PubMed: 19812043]

23. Zhang Y, Yang Y, Hong H, Cai W. Multimodality molecular imaging of CD105 (Endoglin) expression. Int J Clin Exp Med. 2011; 4:32–42. [PubMed: 21394284]

24. Dallas NA, Samuel S, Xia L, Fan F, Gray MJ, Lim SJ, et al. Endoglin (CD105): a marker of tumor vasculature and potential target for therapy. Clin Cancer Res. 2008; 14:1931–7. [PubMed: 18381930]

25. Rosen LS, Hurwitz HI, Wong MK, Goldman J, Mendelson DS, Figg WD, et al. A phase I first-in-human study of TRC105 (Anti-Endoglin Antibody) in patients with advanced cancer. Clin Cancer Res. 2012; 18:4820–9. [PubMed: 22767667]

26. Gambhir SS. Molecular imaging of cancer with positron emission tomography. Nat Rev Cancer. 2002; 2:683–93. [PubMed: 12209157]

27. Alauddin MM. Positron emission tomography (PET) imaging with ^{18}F-based radiotracers. Am J Nucl Med Mol Imaging. 2012; 2:55–76. [PubMed: 23133802]

28. Eary JF, Hawkins DS, Rodler ET, Conrad EUI. ^{18}F-FDG PET in sarcoma treatment response imaging. Am J Nucl Med Mol Imaging. 2011; 1:47–53. [PubMed: 23133794]

29. Grassi I, Nanni C, Allegri V, Morigi JJ, Montini GC, Castellucci P, et al. The clinical use of PET with ^{11}C-acetate. Am J Nucl Med Mol Imaging. 2012; 2:33–47. [PubMed: 23133801]

30. Liu X, Tao H, Yang K, Zhang S, Lee ST, Liu Z. Optimization of surface chemistry on single-walled carbon nanotubes for in vivo photothermal ablation of tumors. Biomaterials. 2011; 32:144–51. [PubMed: 20888630]

31. Hong H, Yang K, Zhang Y, Engle JW, Feng L, Yang Y, et al. In vivo targeting and imaging of tumor vasculature with radiolabeled, antibody-conjugated nanographene. ACS Nano. 2012; 6:2361–70. [PubMed: 22339280]

32. Zhang Y, Hong H, Severin GW, Engle JW, Yang Y, Goel S, et al. ImmunoPET and near-infrared fluorescence imaging of CD105 expression using a monoclonal antibody dual-labeled with ^{89}Zr and IRDye 800CW. Am J Transl Res. 2012; 4:333–46. [PubMed: 22937210]

33. Hong H, Zhang Y, Severin GW, Yang Y, Engle JW, Niu G, et al. Multimodality Imaging of Breast Cancer Experimental Lung Metastasis with Bioluminescence and a Monoclonal Antibody Dual-Labeled with ^{89}Zr and IRDye 800CW. Mol Pharm. 2012; 9:2339–49.

34. Hong H, Zhang Y, Engle JW, Nayak TR, Theuer CP, Nickles RJ, et al. In vivo targeting and positron emission tomography imaging of tumor vasculature with ^{66}Ga-labeled nano-graphene. Biomaterials. 2012; 33:4147–56. [PubMed: 22386918]

35. Zhang Y, Hong H, Engle JW, Yang Y, Barnhart TE, Cai W. Positron Emission Tomography and Near-Infrared Fluorescence Imaging of Vascular Endothelial Growth Factor with Dual-Labeled Bevacizumab. Am J Nucl Med Mol Imaging. 2012; 2:1–13. [PubMed: 22229128]

36. Choi HS, Liu W, Misra P, Tanaka E, Zimmer JP, Itty Ipe B, et al. Renal clearance of quantum dots. Nat Biotechnol. 2007; 25:1165–70. [PubMed: 17891134]

37. Robinson JT, Tabakman SM, Liang Y, Wang H, Casalongue HS, Vinh D, et al. Ultrasmall reduced graphene oxide with high near-infrared absorbance for photothermal therapy. J Am Chem Soc. 2011; 133:6825–31. [PubMed: 21476500]

38. Iagaru A. ^{18}F-FDG PET/CT: timing for evaluation of response to therapy remains a clinical challenge. Am J Nucl Med Mol Imaging. 2011; 1:63–4. [PubMed: 23133796]
39. Vach W, Høilund-Carlsen PF, Fischer BM, Gerke O, Weber W. How to study optimal timing of PET/CT for monitoring of cancer treatment. Am J Nucl Med Mol Imaging. 2011; 1:54–62. [PubMed: 23133795]
40. Zhang Y, Hong H, Engle JW, Bean J, Yang Y, Leigh BR, et al. Positron emission tomography imaging of CD105 expression with a ^{64}Cu-labeled monoclonal antibody: NOTA is superior to DOTA. PLoS One. 2011; 6:e28005. [PubMed: 22174762]
41. Dearling JLJ, Voss SD, Dunning P, Snay E, Fahey F, Smith SV, et al. Imaging cancer using PET -- the effect of the bifunctional chelator on the biodistribution of a ^{64}Cu-labeled antibody. Nucl Med Biol. 2011; 38:29–38. [PubMed: 21220127]
42. Liu Z, Cai W, He L, Nakayama N, Chen K, Sun X, et al. In vivo biodistribution and highly efficient tumour targeting of carbon nanotubes in mice. Nat Nanotechnol. 2007; 2:47–52. [PubMed: 18654207]
43. Cai W, Chen K, Li ZB, Gambhir SS, Chen X. Dual-function probe for PET and near-infrared fluorescence imaging of tumor vasculature. J Nucl Med. 2007; 48:1862–70. [PubMed: 17942800]
44. Cai W, Chen X. Preparation of peptide conjugated quantum dots for tumour vasculature targeted imaging. Nat Protoc. 2008; 3:89–96. [PubMed: 18193025]
45. Cai W, Chen X. Multimodality molecular imaging of tumor angiogenesis. J Nucl Med. 2008; 49(Suppl 2):113S–28S. [PubMed: 18523069]
46. Cai W, Shin DW, Chen K, Gheysens O, Cao Q, Wang SX, et al. Peptide-labeled near-infrared quantum dots for imaging tumor vasculature in living subjects. Nano Lett. 2006; 6:669–76. [PubMed: 16608262]

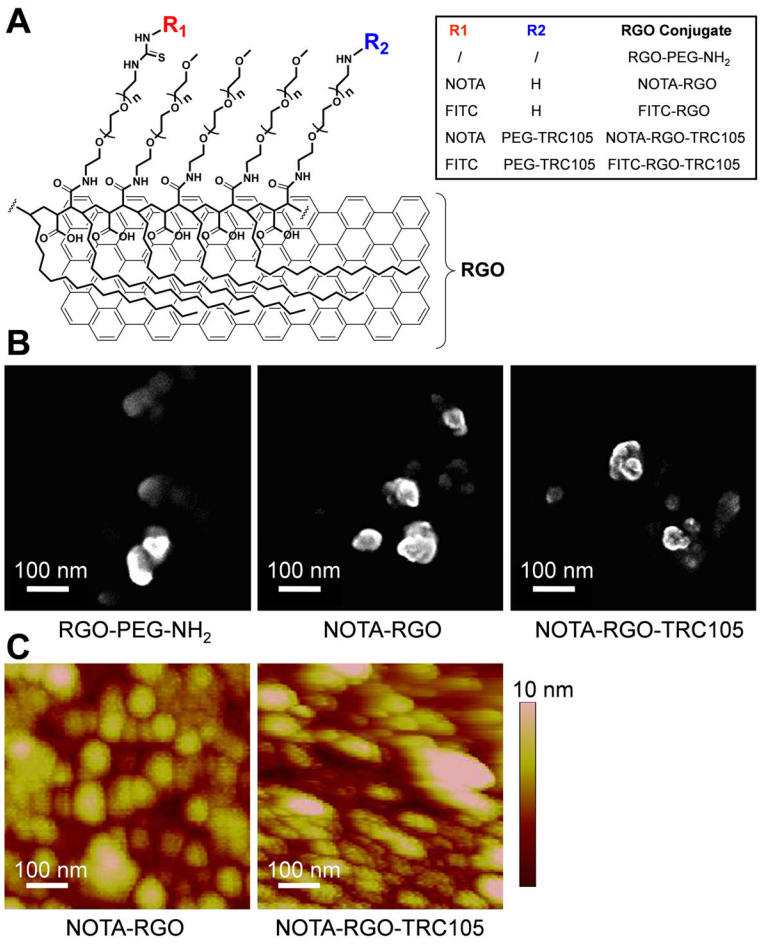

Figure 1.

(**A**) A schematic diagram of the RGO conjugates. (**B**) SEM images of the RGO conjugates. (**C**) AFM images of the RGO conjugates.

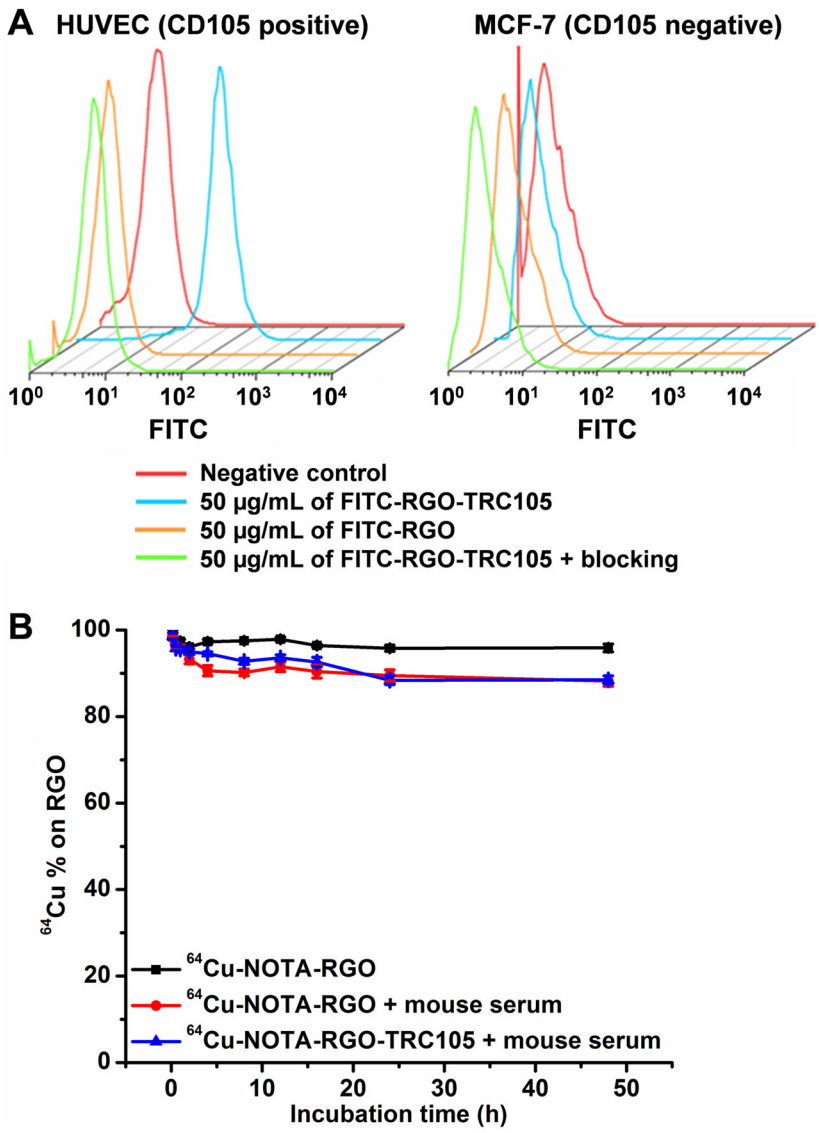

Figure 2.

(**A**) Flow cytometry analysis of the RGO conjugates in HUVECs (CD105 positive) and MCF-7 breast cancer cells (CD105 negative). (**B**) Serum stability studies at 37 °C.

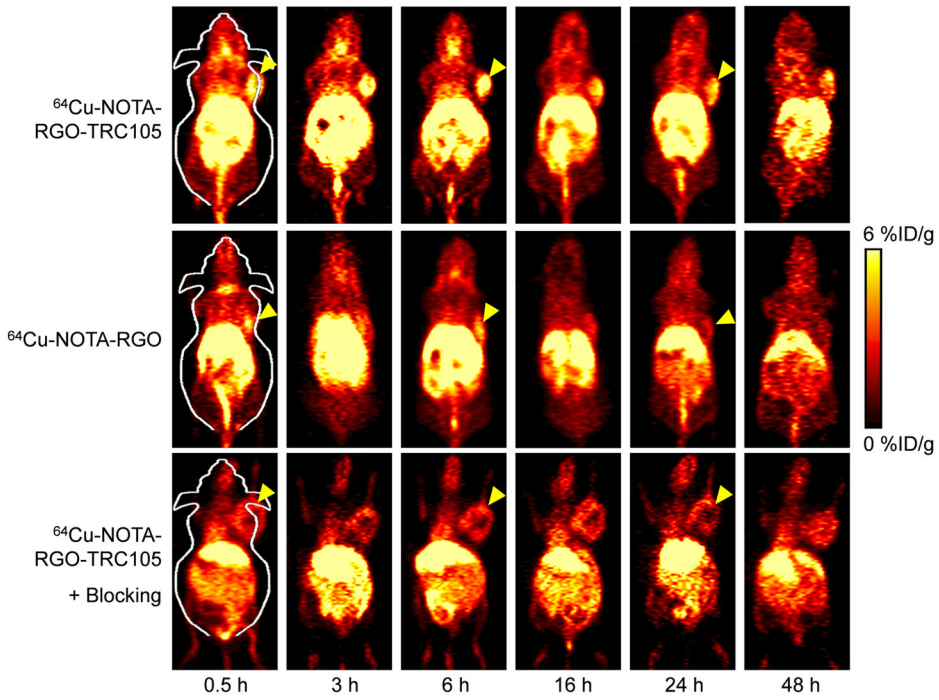

Figure 3.

Serial coronal PET images of 4T1 tumor-bearing mice at different time points post-injection of ^{64}Cu-NOTA-RGO-TRC105, ^{64}Cu-NOTA-RGO, or ^{64}Cu-NOTA-RGO-TRC105 after a pre-injected blocking dose of TRC105. Tumors are indicated by arrowheads.

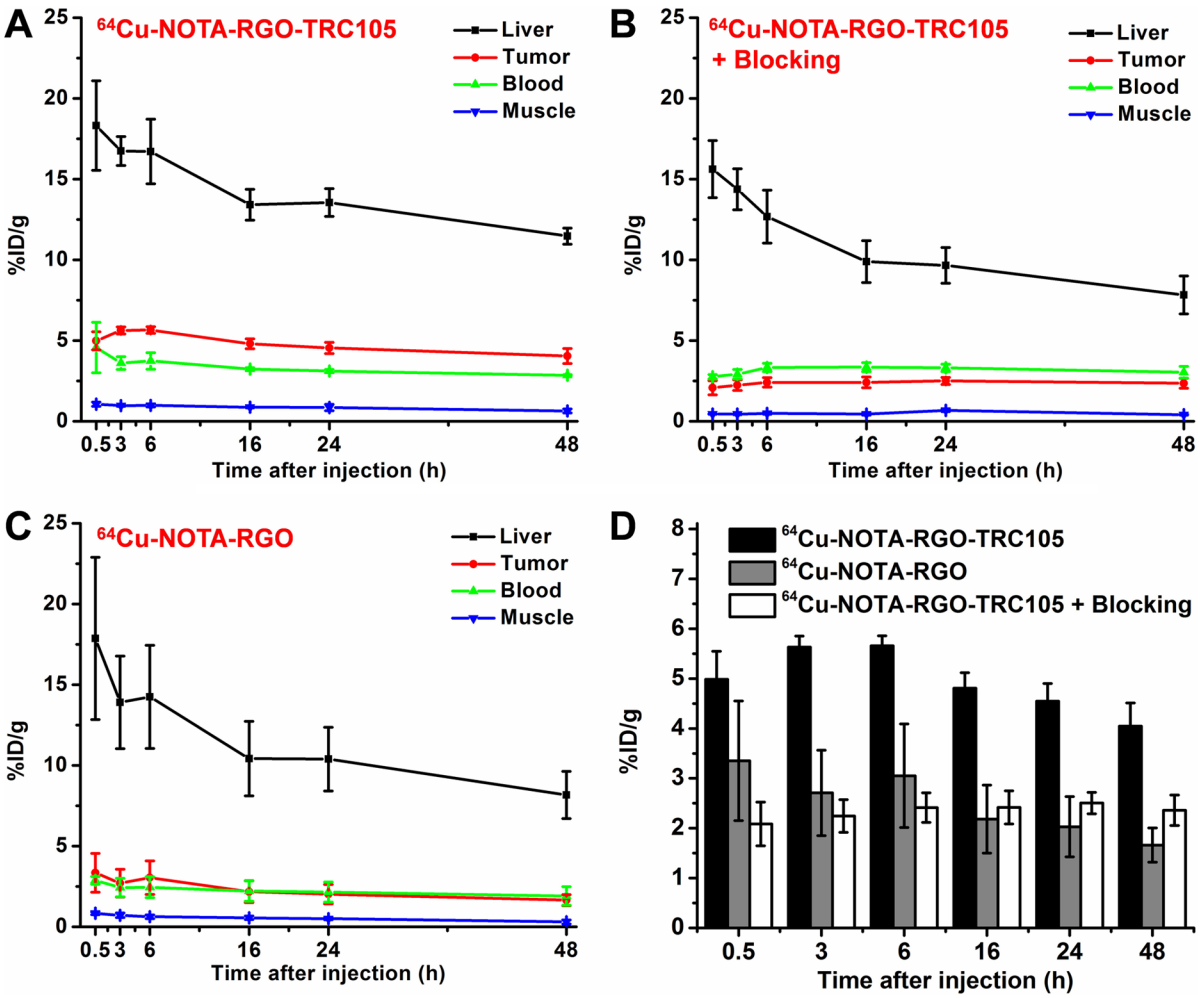

Figure 4.

Quantitative analysis of the PET data. (**A**) Time activity curves of the liver, 4T1 tumor, blood, and muscle upon intravenous injection of ^{64}Cu-NOTA-RGO-TRC105. (**B**) Time activity curves of the liver, 4T1 tumor, blood, and muscle upon intravenous injection of ^{64}Cu-NOTA-RGO-TRC105, after a blocking dose of TRC105. (**C**) Time activity curves of the liver, 4T1 tumor, blood, and muscle upon intravenous injection of ^{64}Cu-NOTA-RGO. (**D**) Comparison of the 4T1 tumor uptake in the three groups. The differences between 4T1 tumor uptake of ^{64}Cu-NOTA-RGO-TRC105 and the two control groups were statistically significant ($P < 0.05$) at all time points, except at 0.5 h post-injection between ^{64}Cu-NOTA-RGO-TRC105 and ^{64}Cu-NOTA-RGO. All data represent 4 mice per group.

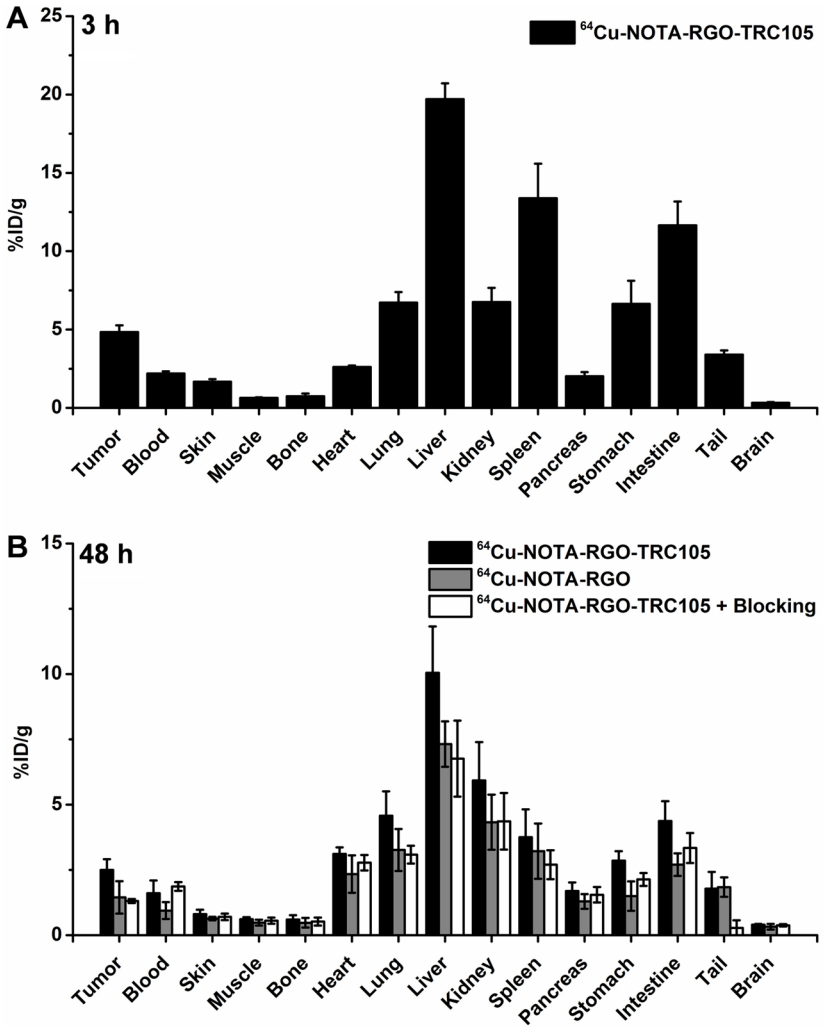

Figure 5.

Biodistribution studies in 4T1 tumor-bearing mice at 3 h (**A**) and 48 h (**B**) post-injection of the RGO conjugates. All data represent 4 mice per group.

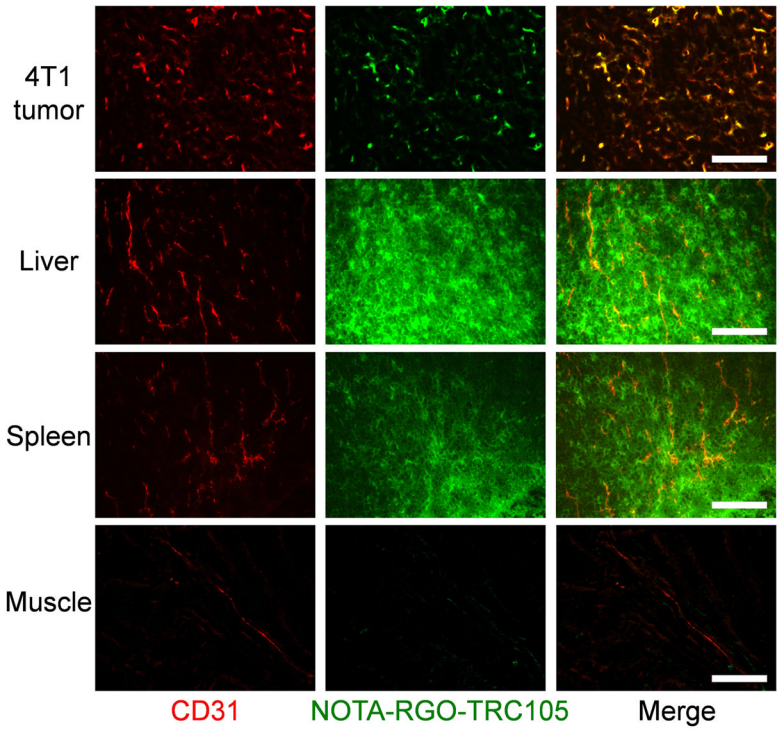

Figure 6.
Immunofluorescence staining of various tissue slices for CD31 (red, with anti-mouse CD31 primary antibody) and CD105 (green, using TRC105 within NOTA-RGO-TRC105 as the primary antibody). Merged images are also shown. Magnification: 200×. Scale bar: 50 μm.